Supporting information

An Antipyrine based Fluorescent Probe for distinct detection of Al^{3+} and Zn^{2+} and Its AIEE Behaviour

Samir Maity, Milan Shyamal, Rakesh Maity, Naren Mudi, Paresh Hazra, Prabhat Kr. Giri, Shashanka Shekhar Samanta, Santanu Pyne and Ajay Misra*

Department of Chemistry, Vidyasagar University, Midnapore 721 102, W.B, India.

Corresponding Author:

E-mail: ajay@mail.vidyasagar.ac.in; Tel.: +91 8967986988; Fax: +91 3222 275329

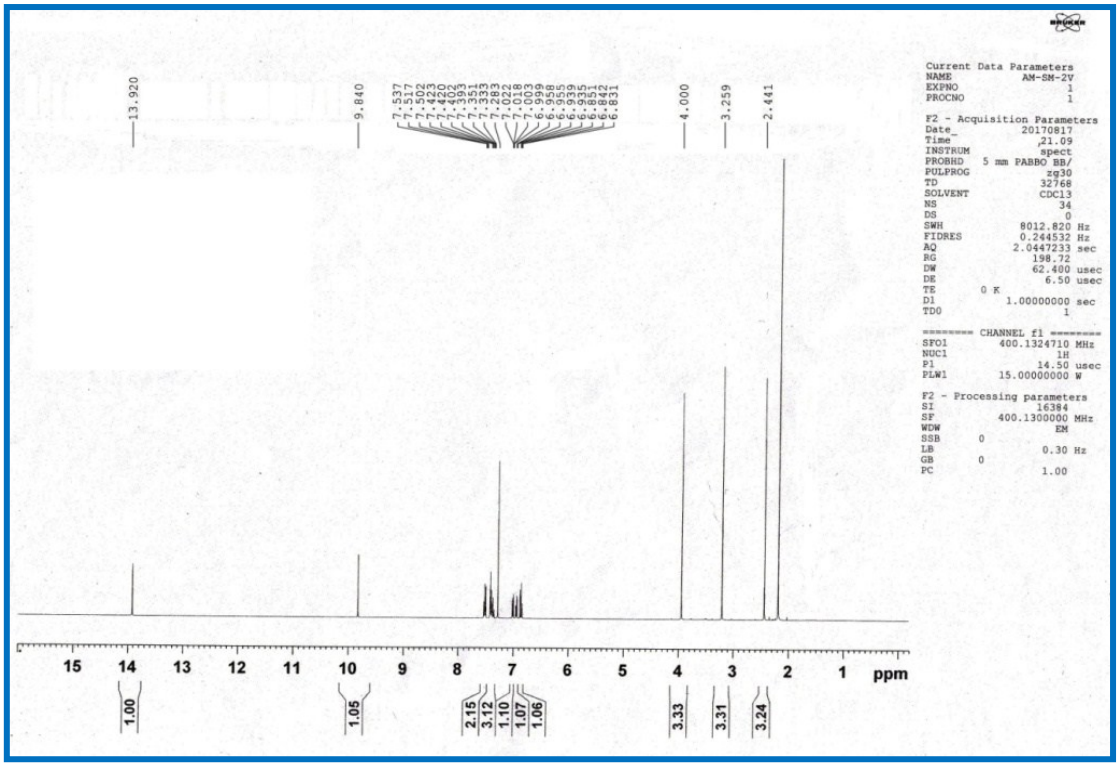

Fig.S1: ^{1}H NMR spectra of OVAP in $CDCl_3$

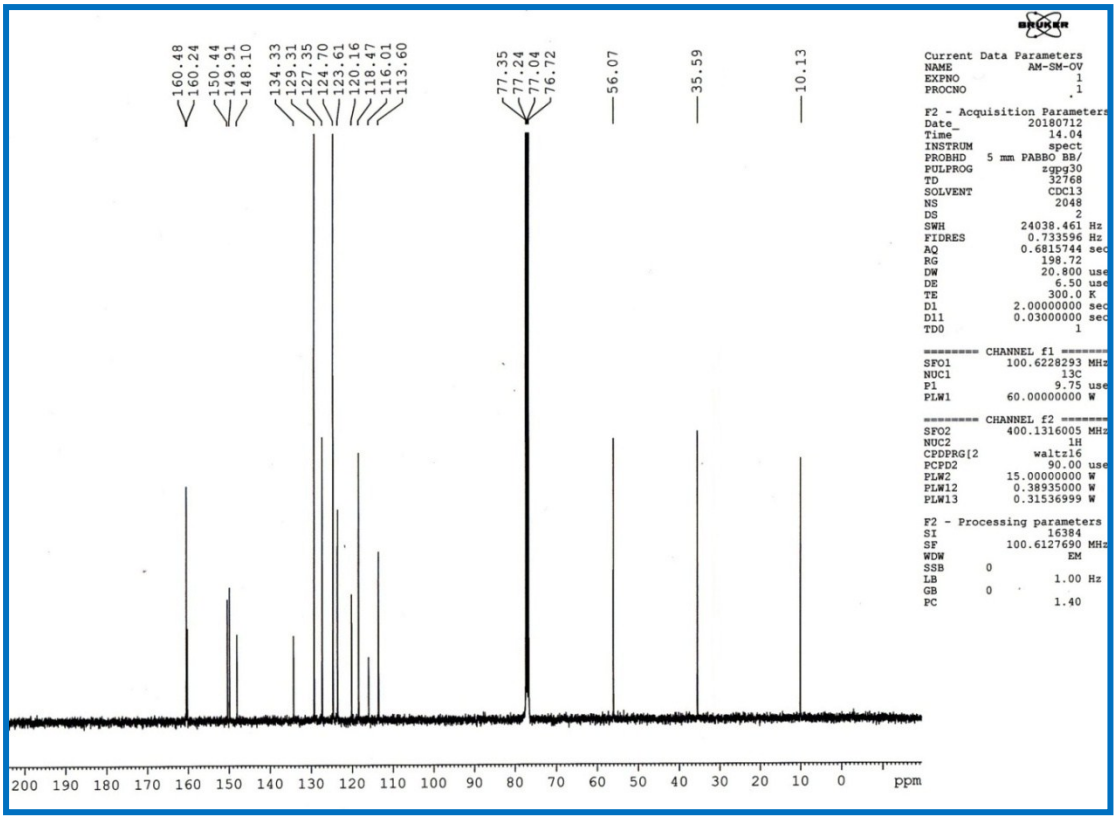

Fig. S2: ^{13}C NMR spectra of OVAP in $CDCl_3$

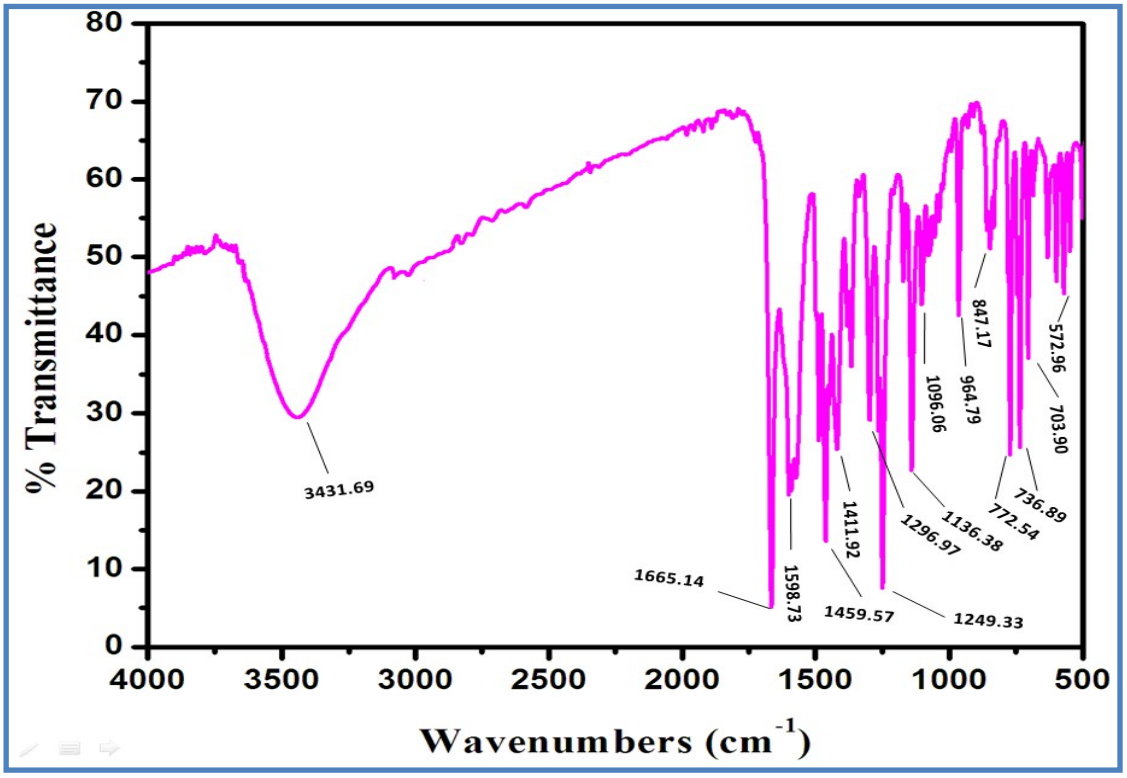

Fig.S3: FT-IR spectra of OVAP

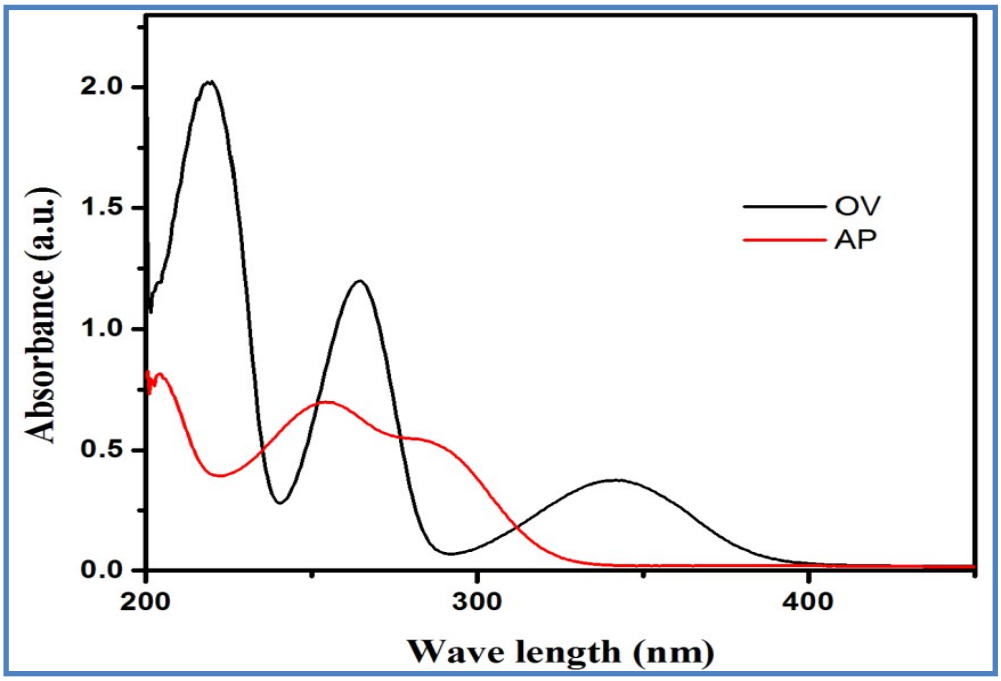

Fig. S4: UV-Vis spectra of O-Vanillin (OV) and 4-aminoantipyrine (AP) in EtOH

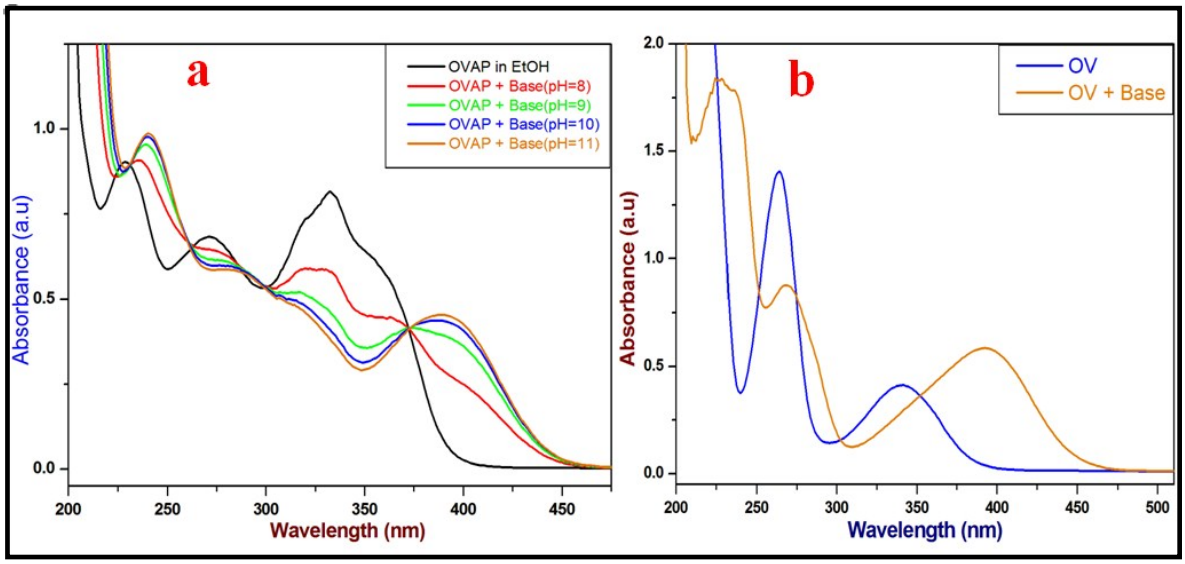

Fig. S5: UV-Vis absorption spectra of (a) OVAP with increasing P^H (b) o-vaniline (OV) in the absence and presence of base ($P^H = 10$)

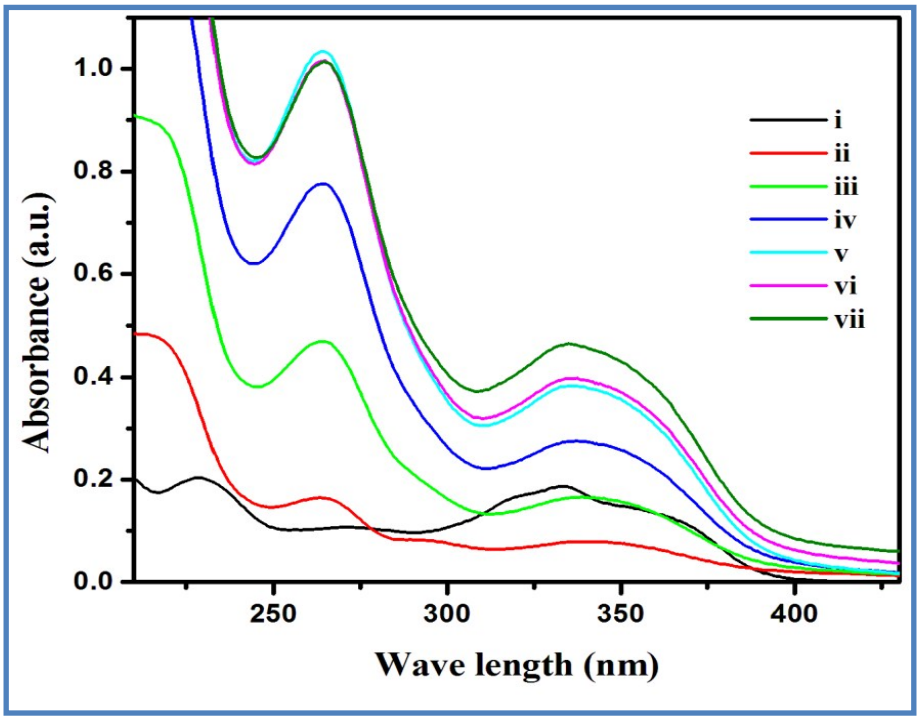

Fig. S6: The UV-Vis absorption spectra of (i) OVAP in EtOH (ii) sample-a, (iii) sample-b, (iv) sample-c, (v) sample-d, (vi) sample-e, (vii) sample-f.

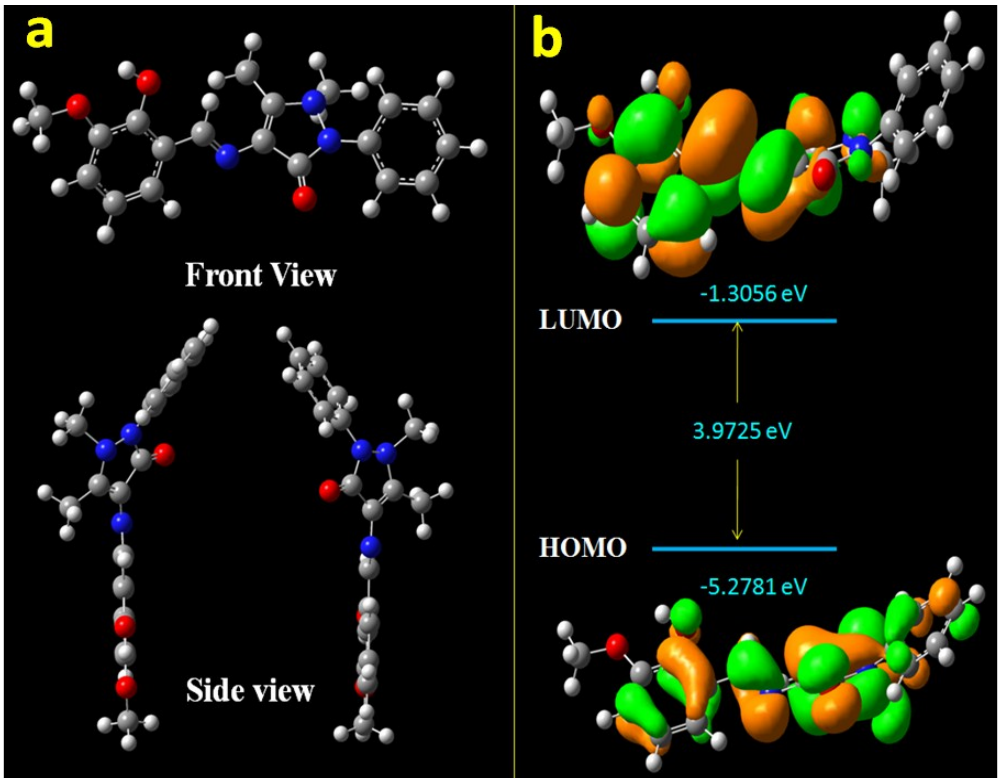

Fig. S7: (a) Optimized structure of OVAP. (b) Frontier molecular orbital plots of HOMO and LUMO energy levels of OVAP calculated by using DFT-B3LYP/6-31 G (d,p) level of theory as implemented on Gaussian 09.

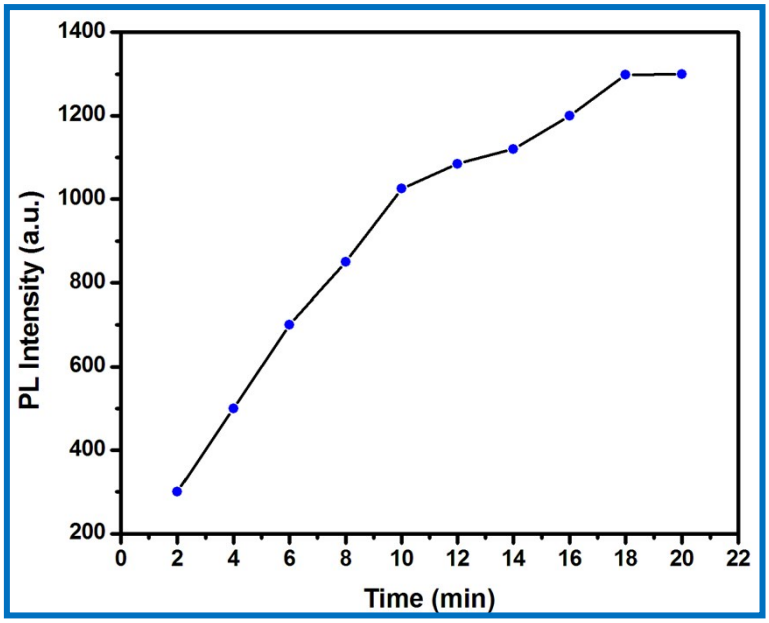

Fig. S8: Time dependent Photophysical study of 99% of OVAP hydrosol.

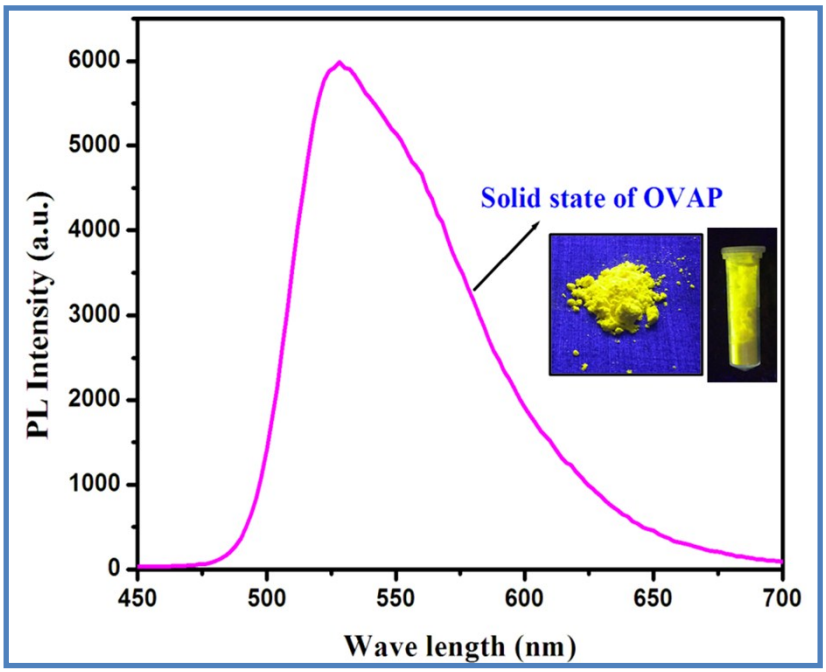

Fig. S9 Solid state emission of OVAP, (Ex-360 nm).

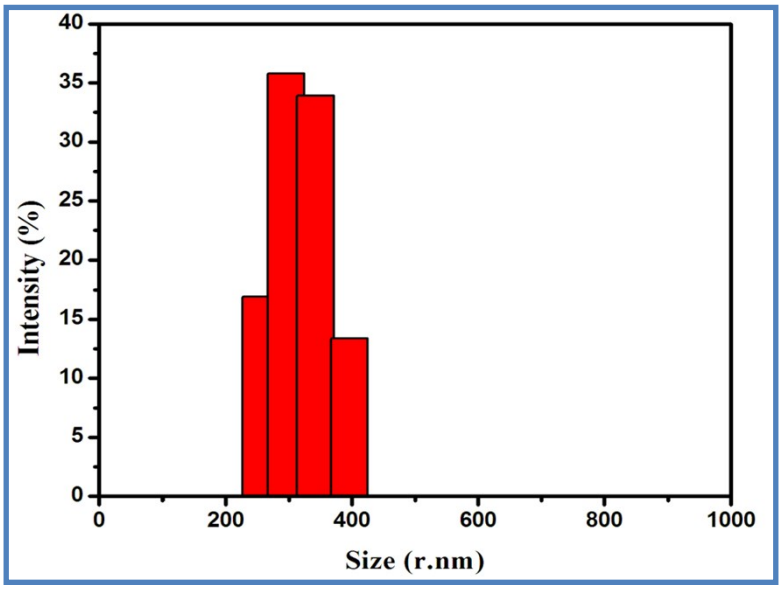

Fig. S10 Particle size distribution of OVAP (47 μM) in mixed aqueous media of 99% water content determined by DLS measurements.

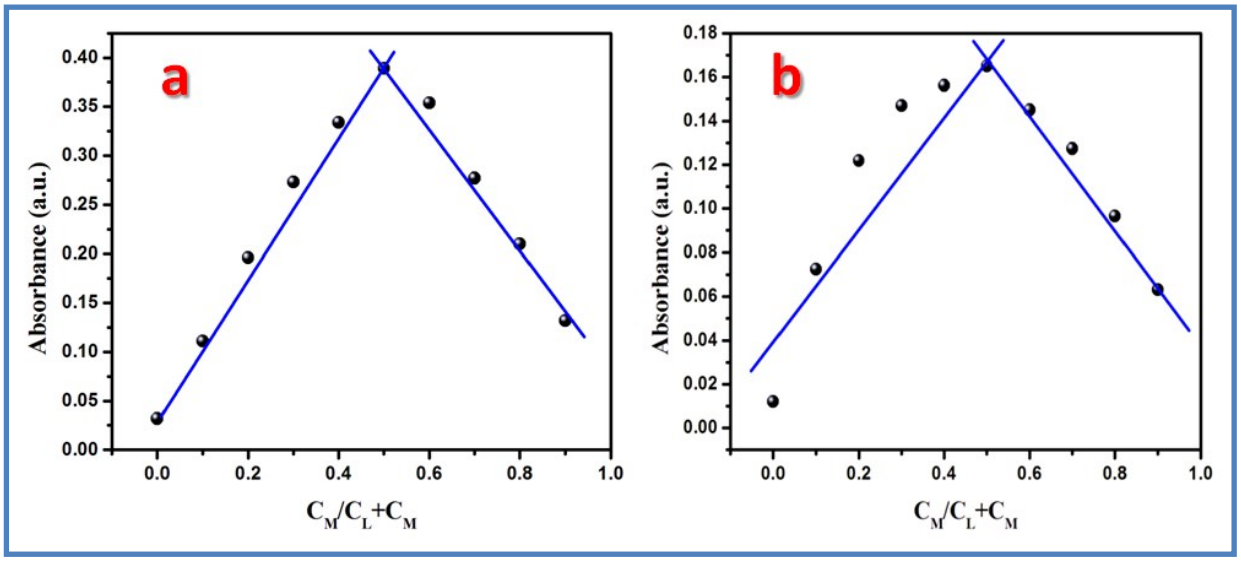

Fig. S11: Job's plot of OVAP in presence of metal ions using continuous variation method, indicating the 1:1 stoichiometry for (a) OVAP–Al^{3+} (b) OVAP–Zn^{2+}.

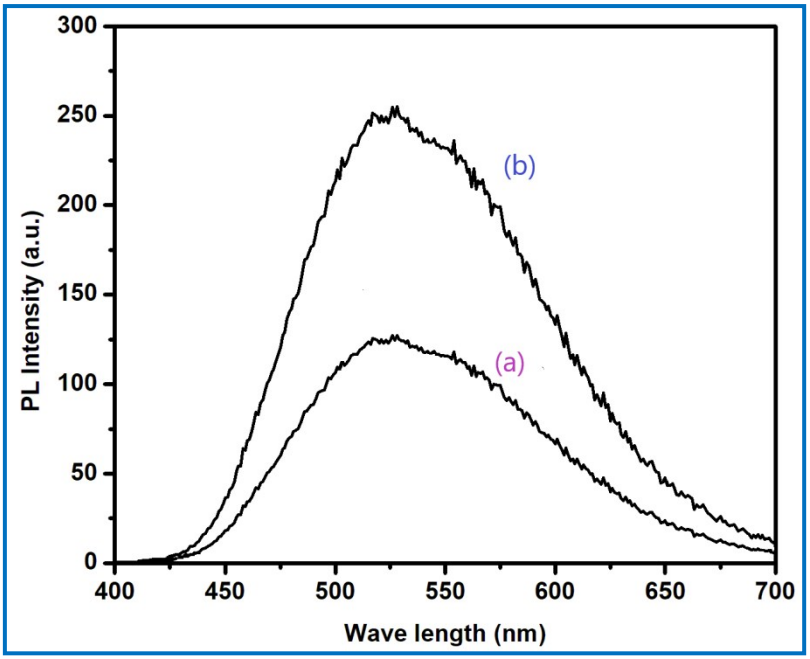

Fig. S12: Fluorescence emission spectra of OVAP (60 mM) in presence of (a) 20 mM each of Al^{3+} & Zn^{2+} , (b) 40 mM each of Al^{3+} & Zn^{2+}.

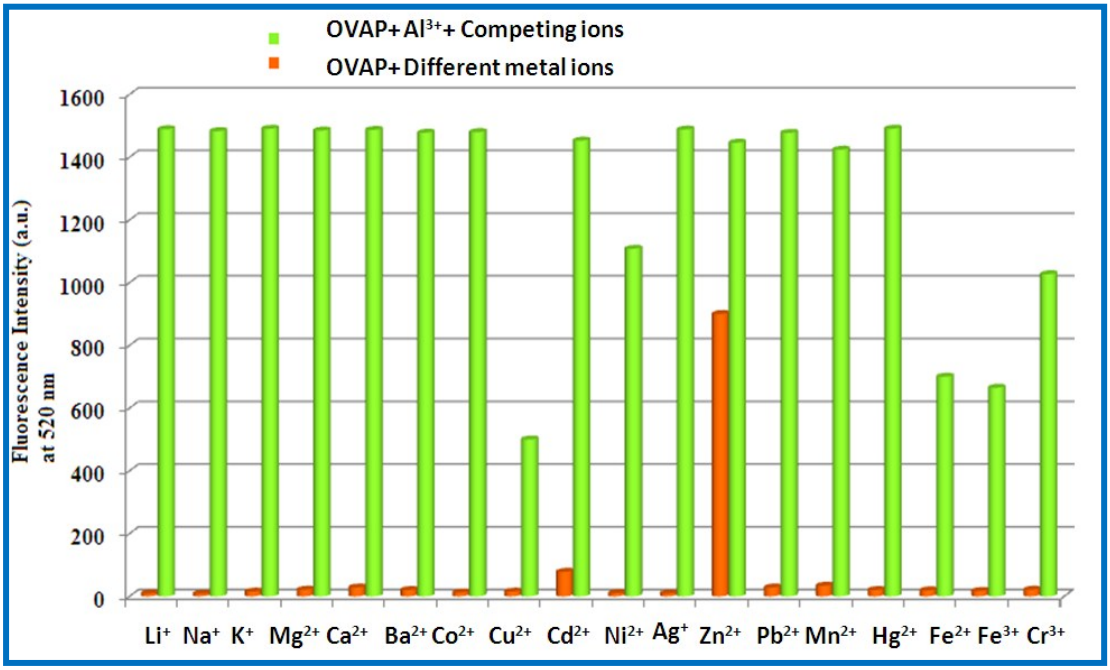

Fig. S13: Selectivity of OVAP for Al^{3+} ions in the presence of other competitive metal ions, excitation wavelength and emission maximum are 360 nm and 520 nm, respectively. Orange bars represent fluorescent intensity after the addition of appropriate metal ion in a 47 µM solution of OVAP. Light green bars represent the subsequent addition of same equiv. of Al^{3+}ions in each of the samples**.**

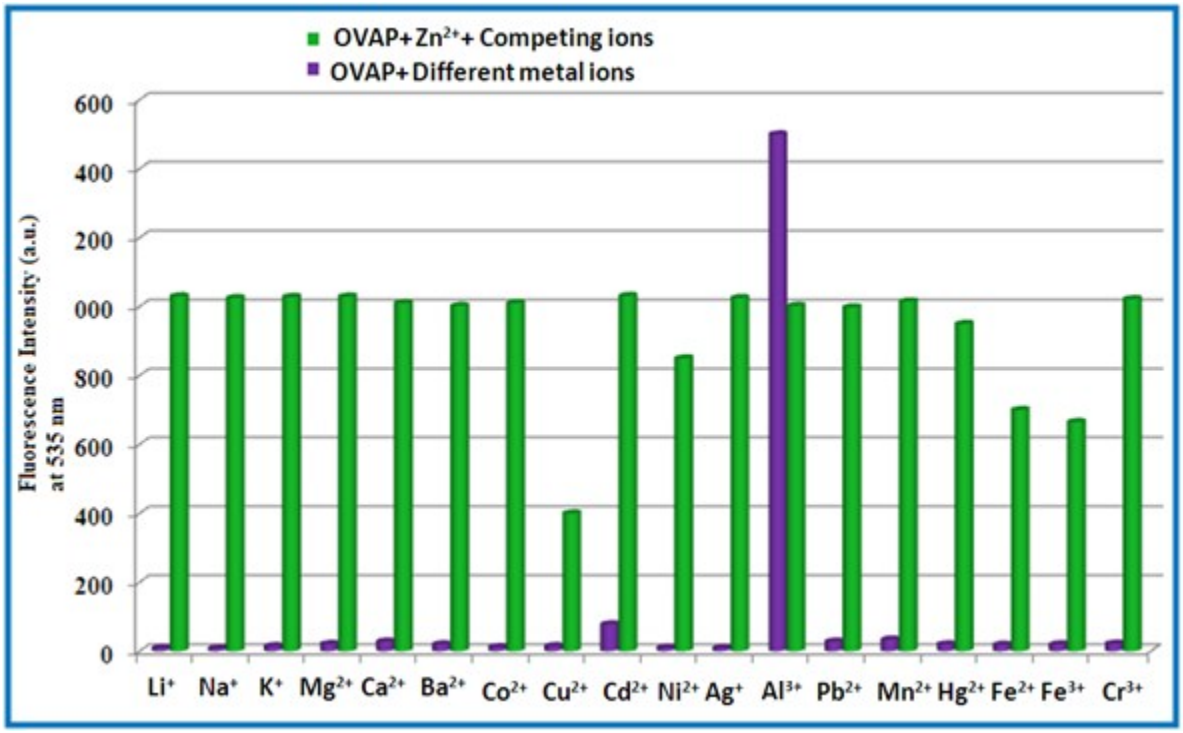

Fig. S14: Selectivity of OVAP for Zn^{2+} ions in the presence of other competitive metal ions, excitation wavelength and emission maximum are 360 nm and 535 nm, respectively. Violet bars represent fluorescent intensity after the addition of the appropriate metal ion in a 47 µM solution of OVAP. Green bars represent the subsequent addition of same equiv. of Zn^{2+} ions in each of the samples.

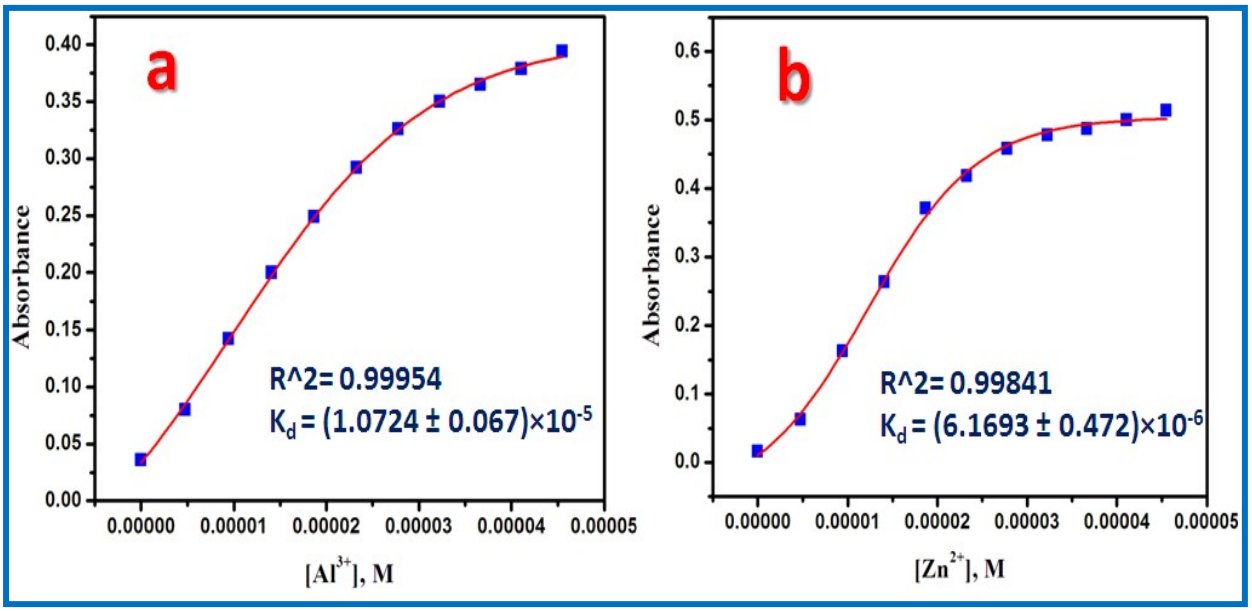

Fig. S15: (a) The plot of absorbance of OVAP-Al^{3+} complex at 405 nm with increasing concentration of Al^{3+} (b) The plot of absorbance of OVAP-Zn^{2+} complex at 425 nm with increasing concentration of Zn^{2+} .

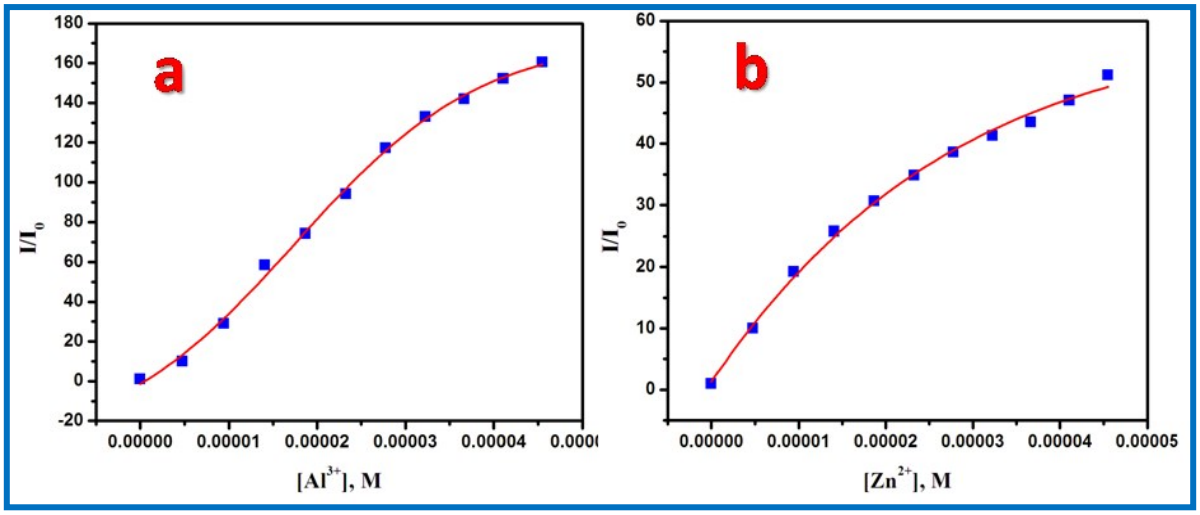

Fig. S16: (a) The plot of normalized emission intensity of OVAP-Al^{3+} complex at 520 nm with increasing concentration of Al^{3+} (b) The plot of normalized emission intensity of OVAP-Zn^{2+} complex at 520 nm with increasing concentration of Zn^{2+} .

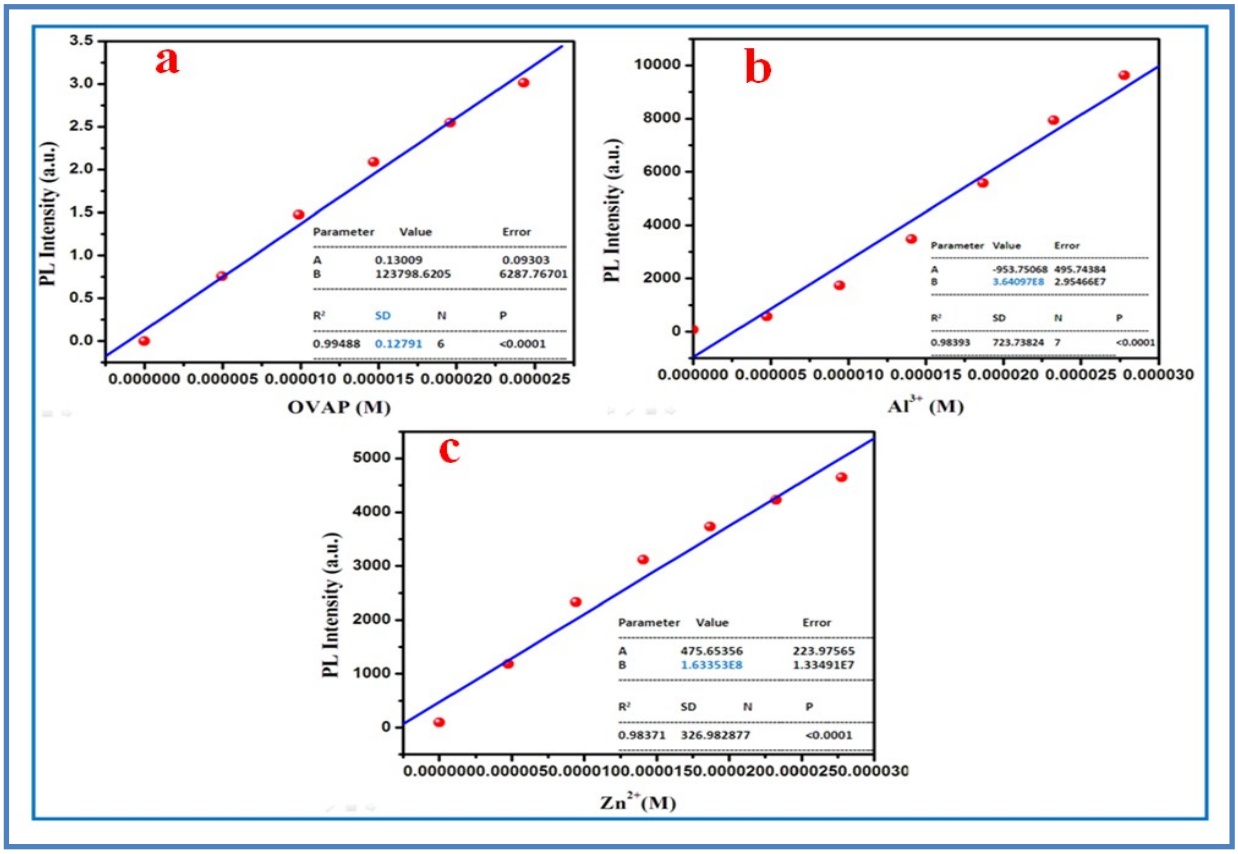

Fig. S17: (a) Plot of fluorescence intensity Vs. concentration of OVAP for measuring standard deviation of LOD experiment; (b) Plot of fluorescence intensity Vs. concentration of Al^{3+} for measuring slope of LOD experiment [LOD (Al^{3+}) = (3 x 0.12791)/3.64097 x 10^8 M = 1.05 x 10^{-9} M] (c) Plot of fluorescence intensity Vs. concentration of Zn^{2+} for measuring slope of LOD experiment [LOD (Zn^{2+}) = (3 x 0.12791)/1.63353 x 10^8 M = 2.35 x 10^{-9} M].

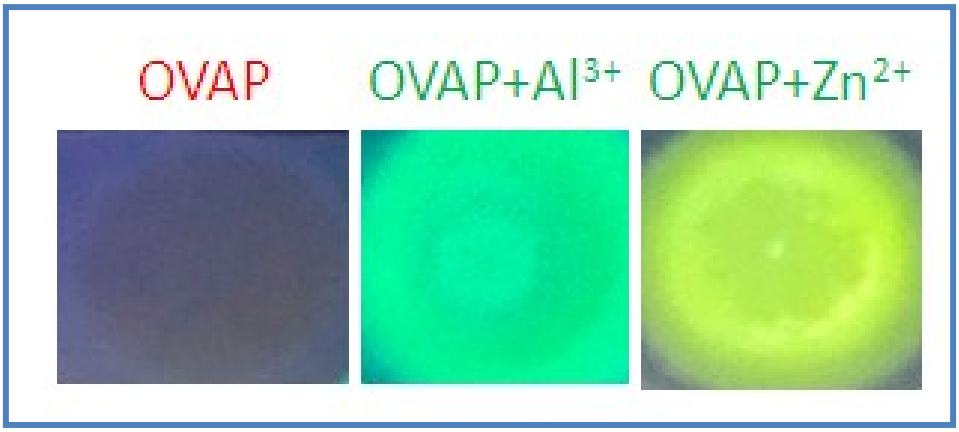

Fig. S18: Photographic fluorescence images of OVAP, OVAP+Al^{3+}, & OVAP+Zn^{2+} under UV light illumination at 365 nm.

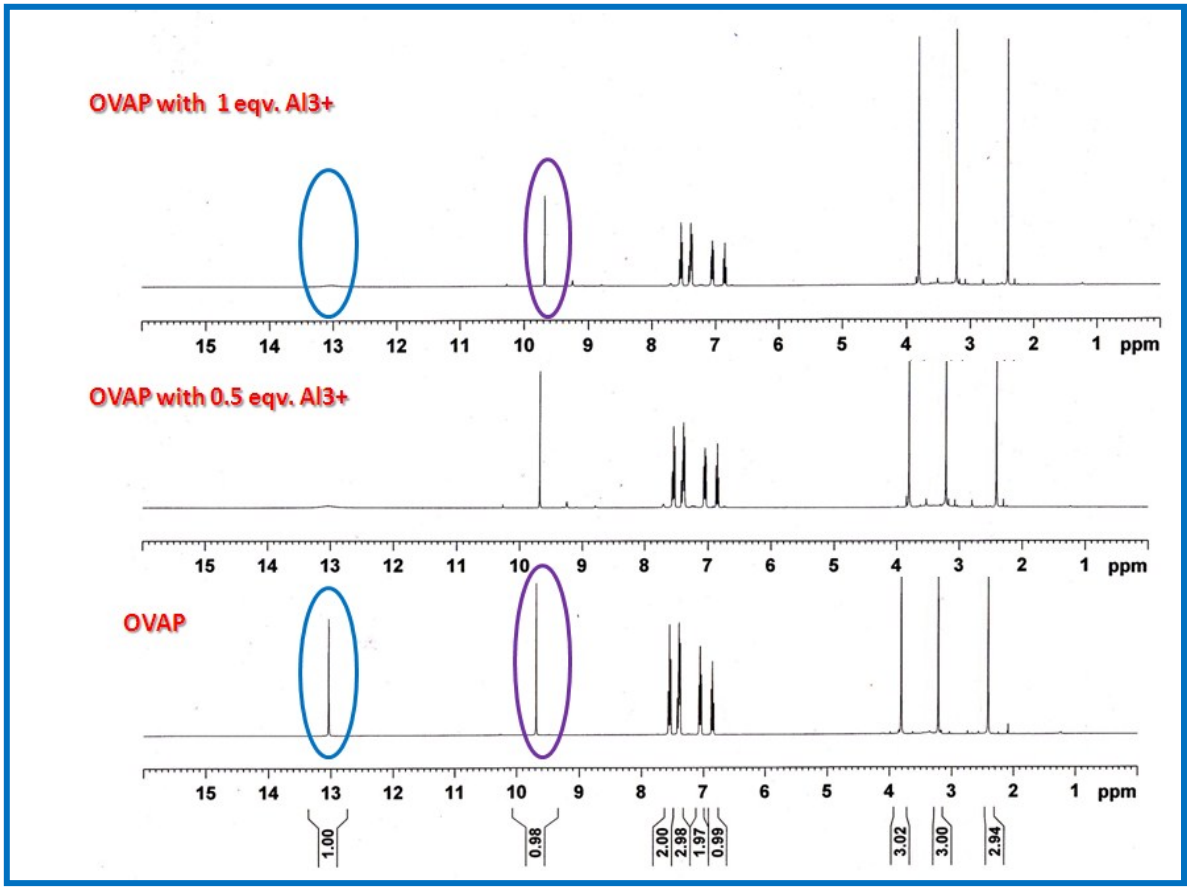

Fig. S19: ^{1}H NMR (400 MHz) spectra of probe OVAP with Al^{3+} (0.0–1.0 eq.) in DMSO-d_6.

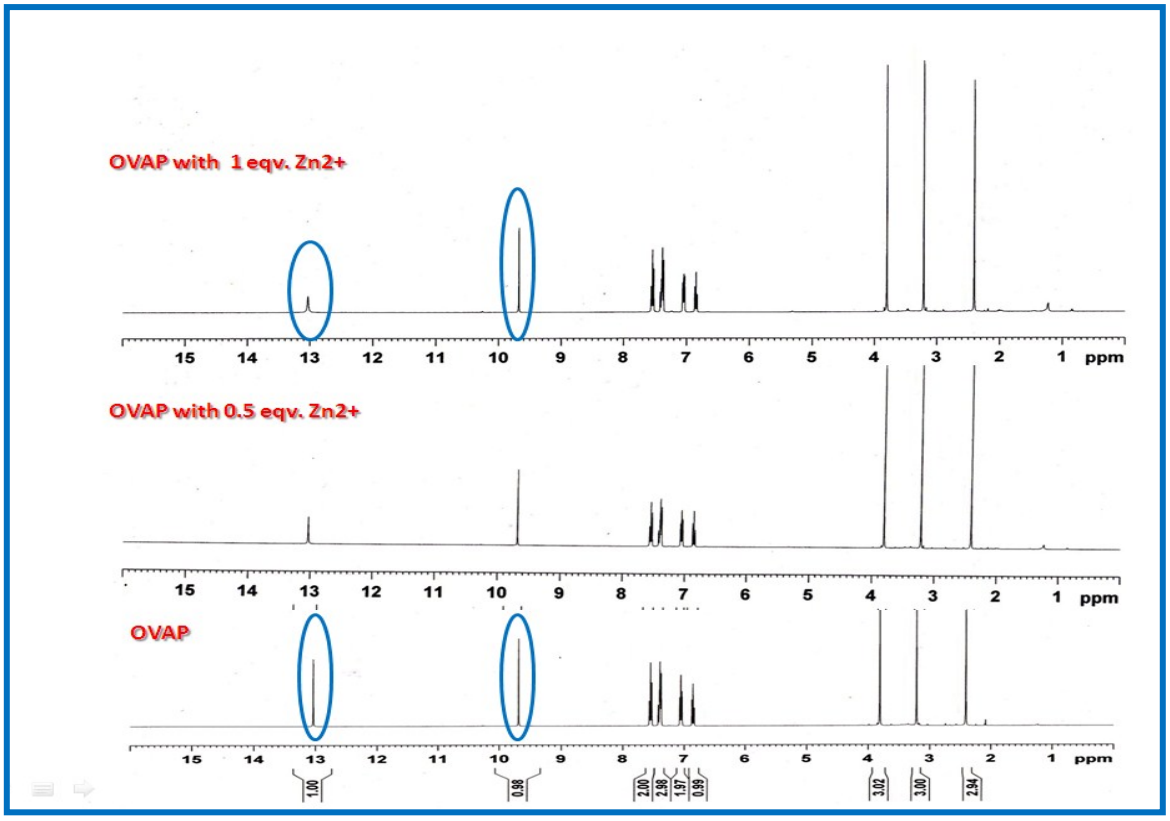

Fig. S20: ^{1}H NMR (400 MHz) spectra of probe OVAP with Zn^{2+} (0.0–1.0 eq.) in DMSO-d_6.

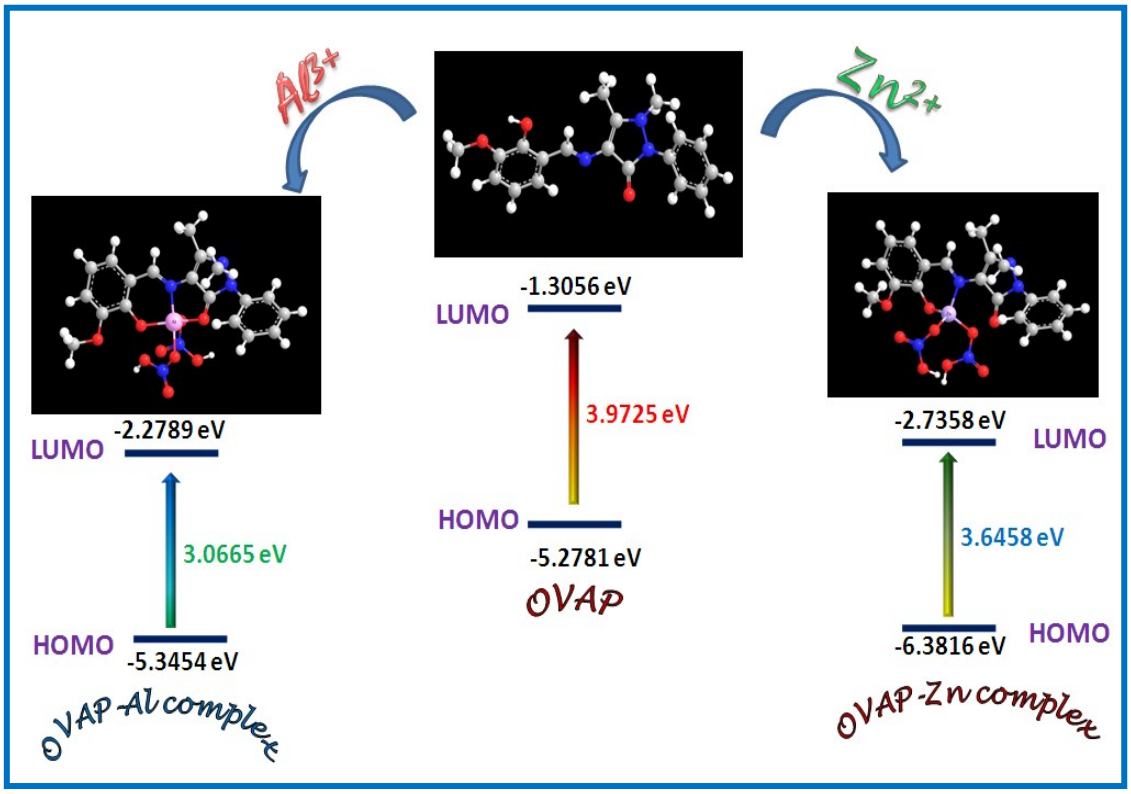

Fig. S21: The optimized geometry of OVAP and its corresponding Al^{3+}, Zn^{2+} complexes along with their HOMO-LUMO energy gap.

Table S1: Comparative Study:

Sl. No.	probe	No. of steps for synthesis	Excitation/ Emission (nm)	LOD (Al^{3+}, Zn^{2+})	DFT study	AIEE property	Solid state study	Ref.
1	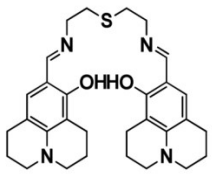	1	355/ 418 (Al^{3+}), 445 (Zn^{2+})	1.34 µM, 1.59 µM	na	na	na	[1]
2	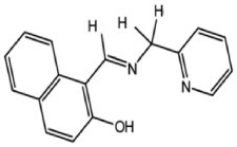	1	370/ 432 (Al^{3+}), 446 (Zn^{2+})	0.648 µM, 1.96 µM	na	na	na	[2]
3	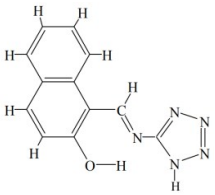	1	420/ 470 (Al^{3+}), 483 (Zn^{2+})	5.86 µM, 1.81 µM	yes	na	na	[3]
4	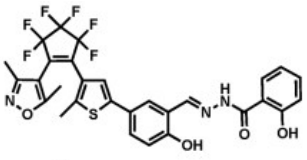	1	372/ 512 (Al^{3+}), 556 (Zn^{2+})	83.10 nm, 0.33 µM	na	na	na	[4]
5	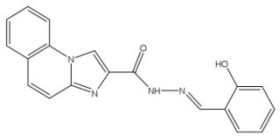	5	305, 315 (Al^{3+}, Zn^{2+}) / 450 (Al^{3+}), 489 (Zn^{2+})	17.3 µM, 0.636 nM	yes	na	na	[5]
6	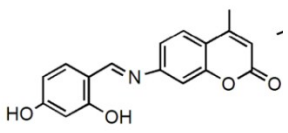	4	357,405 (Al^{3+}, Zn^{2+}) / 427 (Al^{3+}), 496 (Zn^{2+})	3.7 µM, 3.86 µM	na	na	na	[6]

7	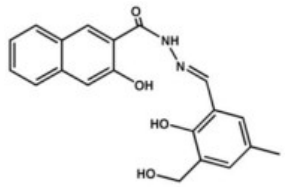	2	398/ 498 (Al^{3+}), 486 (Zn^{2+})	0.92 nM, 3.1 nM	yes	na	na	[7]
8	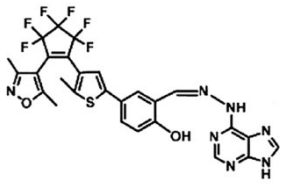	1	370/ 534 (Al^{3+}), 545 (Zn^{2+})	6.7n M, 70.2 nM	na	na	na	[8]
9	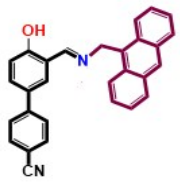	1	365/ 390,410,435 (Al^{3+}), 477 (Zn^{2+})	52.2 nM, 78.8 nM	yes	na	yes	[9]
10	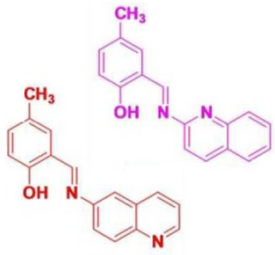	1	330/ 376 (Al^{3+}), 435/550 (Zn^{2+}) 415/ 543 (Al^{3+}), 525 (Zn^{2+})	3.79 , 136.3 nM 23.4, 53.7 nM	yes	na	na	[10]
11	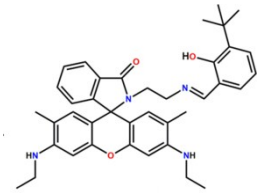	1	500/ 550 (Al^{3+}), 370/457 (Zn^{2+})	10.9 nM 76.9 nM	na	na	na	[11]
12	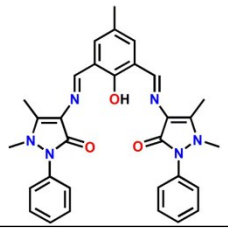	1	390/ 480 (Al^{3+}), 508 (Zn^{2+})	30 nM 21 nM	na	yes	yes	[12]

13	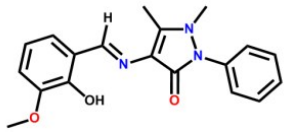	**1**	**360/ 520 (Al^{3+}), 535 (Zn^{2+})**	**1.05 nM, 2.35 nM**	**yes**	**yes**	**yes**	**Present work**

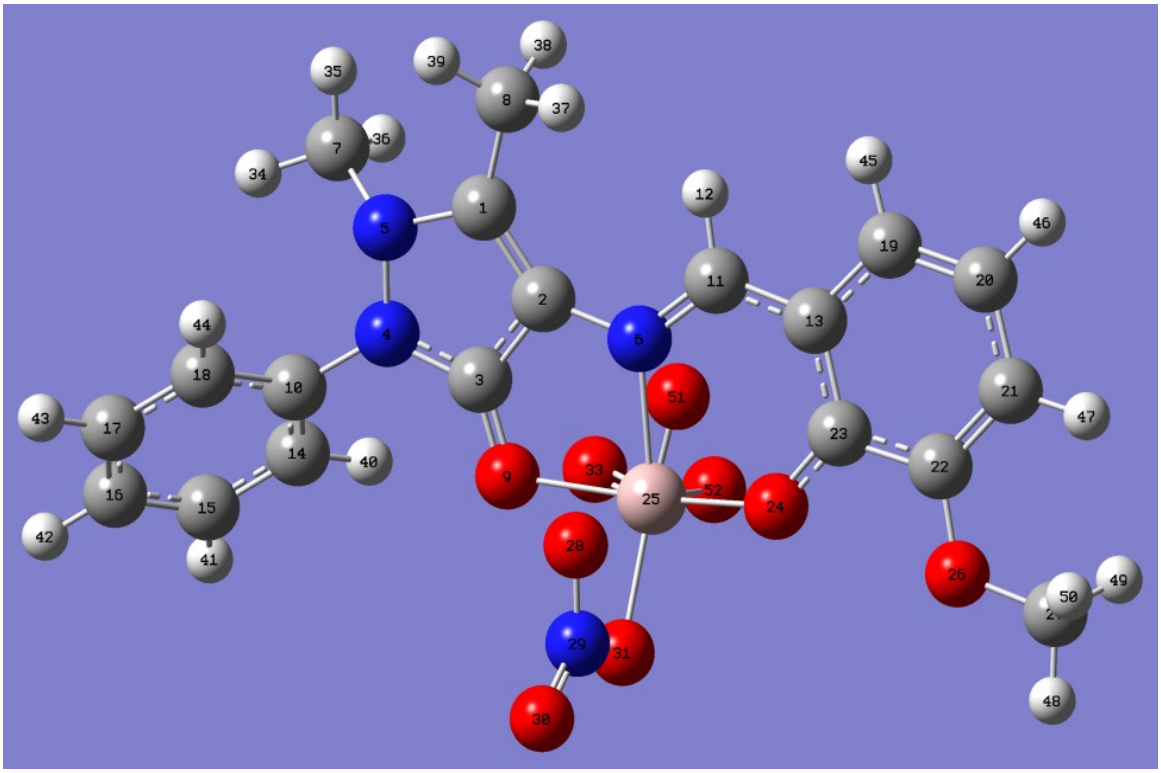

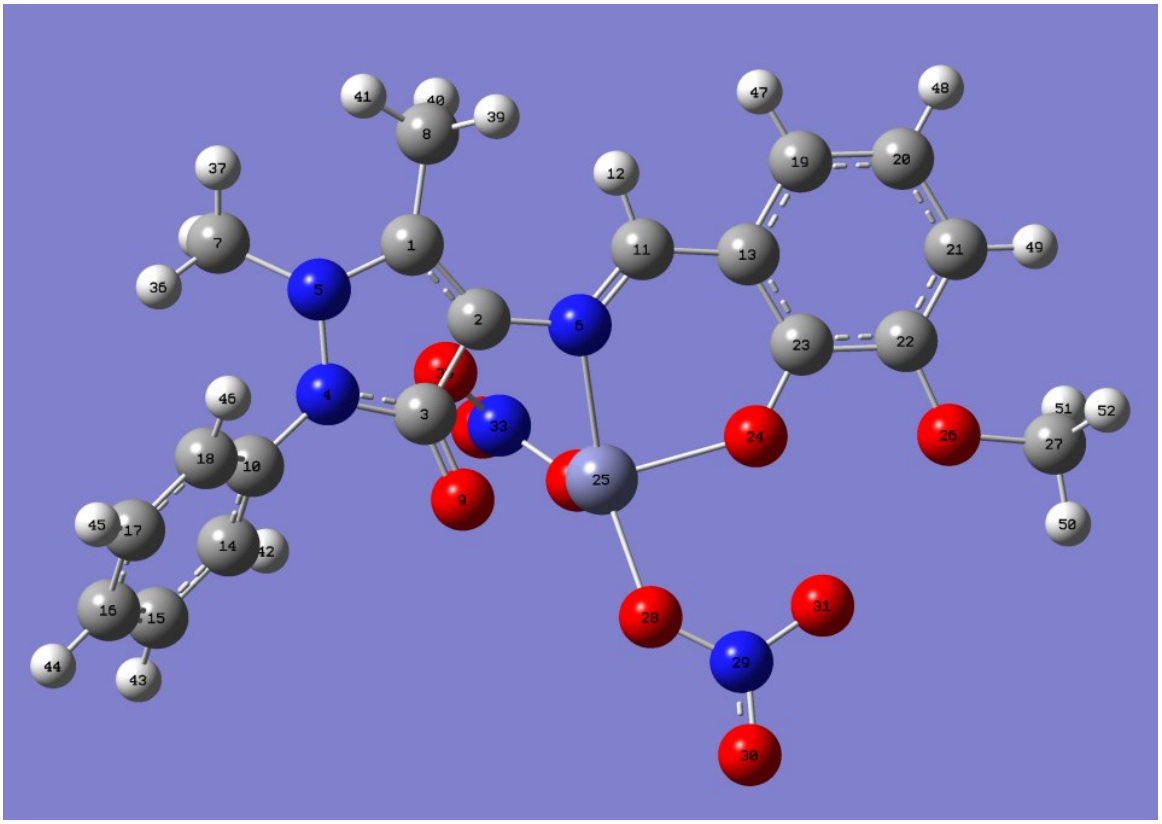

Table S2: Bond distance between metal ions and binding atoms of OVAP in OVAP metal complexes

OVAP-Al^{3+} complex				**OVAP-Zn^{2+} complex**		
Atoms		**Bond distance (A°)**		**Atoms**		**Bond Distance(A°)**
6N	25Al	2.049		6N	25Zn	2.219
24O	25Al	1.832		24O	25Zn	2.096
9O	25Al	1.9923		9O	25Zn	2.088

Reference:

1 Y. S. Kim, G. J. Park, J. J. Lee, S. Y. Lee, S. Y. Lee, C. Kim, Multiple target chemosensor: a fluorescent sensor for Zn(II) and Al(III) and a chromogenic sensor for Fe(II) and Fe(III), *RSC Adv.,* 2015, **5**, 11229-11239.

2 S. Goswami, S. Paul, A. Manna, A differentially selective chemosensor for a ratiometric response to Zn^{2+} and Al^{3+} in aqueous media with applications for molecular switches, *RSC Adv.,* 2013, **3**, 25079-25085.

3 W. H. Ding, W. Cao, X. J. Zheng, W. J. Ding, J. P. Qiao, L. P. Jin, A tetrazole-based fluorescence "turn-on" sensor for Al(III) and Zn(II) ions and its application in bioimaging, *Dalton Trans.,* 2014, **43**, 6429-6435.

4 Y. Fu, Y. Tu, C. Fan, C. Zheng, G. Liu, S. Pu, A highly sensitive fluorescent sensor for Al^{3+} and Zn^{2+} based on a diarylethene salicylhydrazide Schiff base derivative and its bioimaging in live cells, *New J. Chem.*, 2016, **40**, 8579-8586.

5 J. Sun, Z. Liu, Y. Wang, S. Xiao, M. Pei, X. Zhao, G. Zhang, A fluorescence chemosensor based on imidazo[1,2-a]quinoline for Al^{3+} and Zn^{2+} in respective solutions, *RSC Adv*., 2015, **5**, 100873-100878.

6 J. Qin, L. Fan, B. Wang, Z. Yang, T. Li, The design of a simple fluorescent chemosensor for Al^{3+}/Zn^{2+} via two different approaches, *Anal. Methods*, 2015, **7**, 716-722.

7 R. Alam, T. Mistri, R. Bhowmick, A. Katarkar, K. Chaudhuri, M. Ali, ESIPT blocked CHEF based differential dual sensor for Zn^{2+} and Al^{3+} in a pseudo-aqueous medium with intracellular bio-imaging applications and computational studies, *RSC Adv.*, 2016, **6,** 1268-1278.

8 Z. Wang, S. Cui, S. Qiu, S. Pu, A dual-functional fluorescent sensor based on diarylethene for Zn^{2+} and Al^{3+} in different solvents, *J. Photochem. Photobio. A Chemistry*, 2019, **376**,185-195.

9 S. Erdemir, O. Kocyigit, Dual recognition of Zn^{2+} and Al^{3+} ions by a novel probe containing two fluorophore through different signaling mechanisms, *Sens. Actua. B Chem.,* 2018, **273**, 56-61.

10 A. Hazra, A. Roy, A. Mukherjee, G. P. Maiti, P. Roy, Remarkable difference in Al^{3+} and Zn^{2+} sensing properties of quinoline based isomers, *Dalton Trans.,* 2018,**47**, 13972-13989.

11 A. Roy, U. Shee, A. Mukherjee, S. K. Mandal, P. Roy, Rhodamine-Based Dual Chemosensor for Al^{3+} and Zn^{2+} Ions with Distinctly Separated Excitation and Emission Wavelengths, *ACS Omega*, 2019, **4**, 6864−6875.

12 S. Dey, A. Maity, M. Shyamal, D. Das, S. Maity, P. K. Giri, N. Mudi, S. S. Samanta, P. Hazraa, A. Misra, An antipyrine based fluorescence "turn-on" dual sensor for Zn^{2+} and Al^{3+} and its selective fluorescence "turn-off" sensing towards 2,4,6-trinitrophenol (TNP) in the aggregated state *Photochem. Photobiol. Sci.,* 2019, **18,** 2717-2729.